

Article

# Towards Robust and Effective Passive Compliance Design of End-Effectors for Robotic Train Fluid Servicing

Kourosh Eshraghi, Mingfeng Wang \*  and Cristinel Mares

Department of Mechanical and Aerospace Engineering, Brunel University London, London UB8 3PH, UK; kourosh.eshraghi@brunel.ac.uk (K.E.); cristinel.mares@brunel.ac.uk (C.M.)

\* Correspondence: mingfeng.wang@brunel.ac.uk

**Abstract:** Without mechanical compliance robots rely on controlled environments and precision equipment to avoid clashes and large contact forces when interacting with an external workpiece, e.g., a peg-in-hole (PiH) task. In such cases, passive compliance devices are used to reduce the insertion force (and in turn the robot payload) while guiding corrective motions. Previous studies in this field are limited to small misalignments and basic PiH geometries inapplicable to prevalent robotic and autonomous systems (RASs). In addition to these issues, our work argues that there is a lack of a unified approach to the development of passive compliance systems. To this end, we propose a higher-level design approach using robust engineering design (RED) methods. In a case study, we demonstrated this general approach with a Taguchi design framework, developing a remote centre compliant (RCC) end-effector for robotic train fluid servicing. For this specific problem, a pseudo-rigid-body model (PRBM) is suggested in order to save enormous computation time in design, modelling, and optimisation. Our results show that the compliant end-effector is capable of significantly reducing the insertion force for large misalignments up to 15 mm and 6 degrees.

**Keywords:** robotic and autonomous systems; rolling stock maintenance; passive compliance; compliant mechanism; remote centre compliance; robust design; peg in hole



**Citation:** Eshraghi, K.; Wang, M.; Mares, C. Towards Robust and Effective Passive Compliance Design of End-Effectors for Robotic Train Fluid Servicing. *Machines* **2023**, *11*, 997. <https://doi.org/10.3390/machines11110997>

Academic Editor: Alessandro Gasparetto

Received: 30 September 2023

Revised: 19 October 2023

Accepted: 24 October 2023

Published: 27 October 2023



**Copyright:** © 2023 by the authors. Licensee MDPI, Basel, Switzerland. This article is an open access article distributed under the terms and conditions of the Creative Commons Attribution (CC BY) license (<https://creativecommons.org/licenses/by/4.0/>).

## 1. Introduction

Pre-COVID estimates predicted UK rail traffic to surge significantly by 2047, requiring a proportionate increase in the national passenger fleet of between 5500 and 12,000 vehicles, around a 100% increase [1]. More recent post-COVID numbers from the Department of Transport (DoT) show that rail traffic is returning to previous levels. Therefore, estimates of significant growth are certainly back in play. Conversely, new ways of working, such as ‘hybrid’ and ‘work from home’ schemes, will slightly reduce expected peak-time commutes. Regardless of uncertainties, the rail industry seeks to meet higher demand and develop a competitive edge against other modes of transport. Alongside all emerging new technologies for rolling stock and rail infrastructure, RASs have captured our attention. RASs are expanding beyond manufacturing and industrial plants. They will save lives as part of the medical sector and achieve tasks that are difficult or undesirable for humans, e.g., in the hazardous environments of nuclear or space facilities [2,3]. As our society progresses, more repetitive, dirty, or out-of-hours heavy industrial tasks will see labour shortages. RASs will improve work efficiency and reliability, hence many industries such as rail are actively seeking new RASs. Consider, for example, robotic train fluid servicing, which can increase depot capacity, and reduce running costs and the need for new depots to meet future demand [4,5].

The key challenge arises from the accuracy and speed limitations of existing industrial robots in autonomous positioning within outdoor, unstructured, and semi-unstructured environments [6]. These tend to be the environments in which train maintenance is conducted [7]. High-throughput and tight-tolerance tasks tend to be engineering-related, for

example, coupling, assembly, or replacing of mechanical parts, common to many RAS applications. For example, in manufacturing assembly [8] and prevailing applications in automated aeroplane fuselage assembly [9], autonomous satellite servicing [10,11], car refuelling, and in our specific case train fluid servicing [5,12]. Considering our previous work and the existing literature, robot compliance seems the most common and cost-effective method of fast robot alignment for train maintenance. In the following, we discuss existing issues around compliance design and how our proposed approach will contribute.

The relationship between the motion and forces generated by a robotic manipulator and an external part at their point of contact (e.g., end-effector) is defined as robot compliance. This can be divided into two categories, where passive compliance is defined as intrinsic structural deflections such as the flexibility of the robot, while active compliance is achieved by controlling robot actuators and servo motions [13]. Active compliance is easily reprogrammed for a range of tasks, reducing the physical elements and their corresponding complexities. However, it also presents disadvantages, such as relatively slow dynamic responses and a reliance on sophisticated sensors and control systems, which can result in a complex and expensive system. On the other hand, passive compliance is an inherent mechanical capability, considered more reliable, faster in operation, and cheaper to manufacture [14]. These qualities are better suited for high-throughput applications that seek economic efficiency, such as train maintenance. Compliant mechanisms are inherently elastic and underactuated, naturally providing an arbitrary amount of passive compliance [15]. Despite this, they must be designed to guarantee compliance performance to a required degree. The pioneering work in manufacturing PiH assembly [16,17] discusses compliant wrists with RCC, accommodating certain misaligned shaft-bearing (PiH) insertions. Compliance in other robotics, actuators, joints [18,19], or manipulators [20,21], absorb unexpected crashes and improve safety. Compliant and soft grippers adapt to a range of object shapes or provide gripping despite misalignments [22–24]. There are also various applications in minimally intrusive surgeries [25,26], exoskeletons [27], and prosthetics [28] which accommodate unexpected human behaviour or various body part shapes. PiH insertions are the topic most related to train fluid servicing, which requires the assembly of fluid couplers. Achieving the coupling at high speed and low insertion force is the key to meeting the economical requirements of the rail industry. However, as we delved further into the existing literature, we observed idealised mating geometries, represented as either simple cylinders or squares [8,9,29–31]. This is far too rudimentary to represent train fluid ports with mechanical features for sealed, secured, and high-pressure flows. Furthermore, previous studies have proposed analytical models that only predict the insertion force over a small range of misalignments (typically under 2 mm in parallel and a 1° angle) [9,16,31,32]. This is not very useful for unstructured outdoor conditions that impose larger uncertainty in robot sensor measurements. Consequently, designers may resort to trial-and-error approaches with FEA. Due to the dynamic nature of the problem, which includes nonlinear contact and large deformations, such FEA models will be very time consuming and difficult to run.

Beyond these specific issues with the PiH problem, we have noticed another more general pattern across the literature on passive compliance devices [16–28]. The structure of papers follows a common approach where, due to a specific problem, a compliant mechanism is synthesised, modelled, and analysed to showcase its performance for the intended task. This is great, but it does not guarantee or make clear how we may implement that approach for innovative solutions to new problems. This level of guidance is only useful when working with the same design form within similar parametric and application limits. Based on our experience, such a scenario is a rare luxury in the development of new RAS in outdoor and unstructured environments. Accordingly, there is a need for a unified and generalised compliance design approach.

Inspired by RED methodologies [33,34], we demonstrate a new outlook which distinguishes compliance design through the existence of certain uncertainties. This has resulted in a higher-level design framework that is independent of design forms, models, applica-

tions, or parametric limits. We further claim contribution in implementing the methodology for developing an RCC end-effector in new train maintenance applications. This includes modelling the insertion force within the complicated PiH problem where, as compared to finite element analysis (FEA), the suggested PRBM approach reduces computational costs by orders of magnitude. We have not found these didactics in the existing literature.

In Section 2, we introduce and discuss the general methodology. Subsequent subsections delve into the train fluid servicing case study within a classic design process, demonstrating how to ensure compliance with specifications. Section 3 covers an illustration and discussion of the case study results. Lastly, in Section 4, we discuss and conclude the key outcomes and subtleties.

## 2. Materials and Methods

### 2.1. The Proposed Approach

Passive compliance design problems in this work can be distinguished by the existence of some kind of uncertainty, which manifests itself through the force–displacement relationship at the point of contact between a robot and an external workpiece. Uncertainties between mating parts may include misalignments, geometrical dimensions, surface finish (friction), etc. Hereafter, these are referred to as noise factors. The compliant mechanism must convert all mechanical inputs into feasible output loads and displacements, which in turn achieve a task, delivering performance. In passive compliance applications, this is usually regulating forces, providing guiding motions, or transferring the load. Such quantifiable performance measures will be referred to as responses. The geometry, dimensions, topology, and material properties of the mechanism are controllable factors that are set by the designer. Hereafter, these are referred to as design factors. In some form or another, design and noise factors are related to the compliance performance of the mechanism; see Figure 1. There must also exist a set of design factors (a design configuration) which minimises the effect of all uncontrollable noise factors on the response. If we can identify this set and ensure the response meets our pre-specified requirements, we have solved the design problem and ensured robustness too.

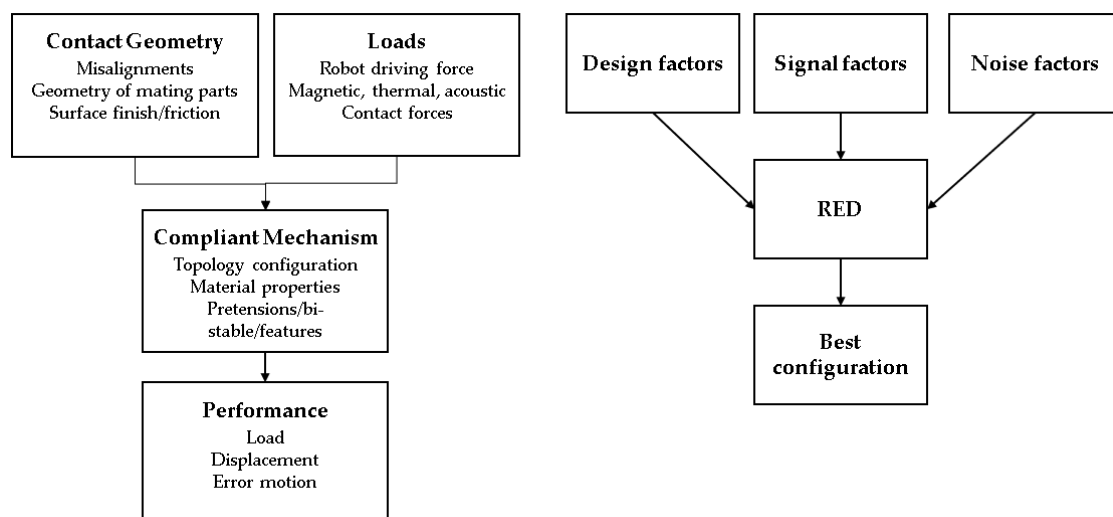


**Figure 1.** Inputs and outputs of compliant mechanism in passive compliance (left), inputs and outputs of robust engineering design methods (right).

Generally, RED aims to minimise performance variance (or standard deviation (SD)) and maximise performance mean. This is subject to a feasible interval of design factors

and possible noise. This may be formulated as a multi-objective optimisation problem as shown below:

$$\begin{aligned} & \min(\bar{Y}, Y_{SD}) \\ & \text{Subject to :} \\ & \mathbf{x}_{\min} \leq \mathbf{x} \leq \mathbf{x}_{\max} \\ & \mathbf{z}_{\min} \leq \mathbf{z} \leq \mathbf{z}_{\max} \end{aligned} \quad (1)$$

where  $\bar{Y}$  and  $Y_{SD}$  are, respectively, the mean and standard deviation for performance.  $\mathbf{x}$  and  $\mathbf{z}$  are the design and noise factors, respectively.

Since we are interested in the design configuration which results in the best mean and SD, these two quantities are calculated at every design configuration across the noise variables.

$$\bar{Y} = \frac{1}{n} \sum_{i=1}^n Y_i \quad (2)$$

$$Y_{sd} = \sqrt{\frac{\sum_{i=1}^n (Y_i - \bar{Y})^2}{n - 1}} \quad (3)$$

where  $Y$  is the observed value for the given design configuration, and  $n$  is the number of performance evaluations across the set of noise configurations.

The above can be satisfied through a series of tests that may be structured through many approaches. Ref. [34] illustrates this for design of experiments (DoEs), Ref. [33] makes a comparison between DoEs and genetic algorithms (GAs). There are other approaches such as sensitivity-based optimisation or the Taguchi method [35], which can be considered the simplest approach. Regardless of how the tests are structured, the classification of the performance measure  $Y$  will be common to any approach. This should be established as a specification metric or requirement. In the case of passive compliance applications, we have categorised them as listed below.

Force regulation and accommodation:

Given an uncertain input load or displacement, a particular force quality (e.g., force in a particular direction) must be controlled. For example, in PiH problems the aim is to reduce the insertion forces during the task, i.e.,

$$Y = F_z \quad (4)$$

where  $F_z$  is a force in a particular direction, in this example the  $z$ -direction.

Load/displacement transfer:

Given an uncertain input, some amount of output displacement or load is required. In such cases we may look at the quantity at the output port of the mechanism, in which case the performance measure looks like Formula (4). However, it may be more beneficial to control the load transfer efficiency and geometrical and mechanical advantages. In compliant mechanism design, transfer efficiency avoids unnecessary strain energy storage. Hence, as an example, any one or all of these metrics may be optimised for

$$Y = \left[ -\frac{d_{\text{out}}}{d_{\text{in}}}; -\frac{F_{\text{out}}}{F_{\text{in}}}; -\frac{F_{\text{out}}d_{\text{out}}}{F_{\text{in}}d_{\text{in}}} \right] \quad (5)$$

where  $d$  denotes displacement and  $F$  denotes force. The subscripts denote the input (in) or output (out) port of the mechanism. From right to left, the 3 expressions are geometric advantage, mechanical advantage, and efficiency. The negative sign changes the minimisation problem to maximisation.

Displacement function, path, or motion generation:

Given a certain input load or displacement, the mechanism's output port should move according to a function or path. In this case, the displacement error (perhaps a sum of errors) to the path or function would be the performance measure, i.e.,

$$Y = \sum_{i=1}^p (d_{\text{out},i} - d_{\text{target},i})^2 \quad (6)$$

where  $d_{\text{target},i}$  is the target displacement at precision point  $i$ . There are  $p$  precision points that approximate the desired output function from a given load.

Any other set of measurable performance measures can be considered. When implemented within a general design procedure [36], the proposed RED approach will result in a very general method of passive compliance design, not bounded by a particular geometry or misalignment limit. This remains practically true for as long as it is possible to feasibly evaluate the performance many times over, satisfying the search nature of the process. As the number of design and noise factors increases, the design space will also expand. In most search algorithms, this tends to increase the number of tests, and the time and effort required. Hence, modelling becomes a crucial part of this process which will be dependent on the exact problem. Maintaining generality, we follow a typical design process of defining, designing, modelling, and testing [36]; see Figure 2. The first step is to investigate the requirements to understand the mechanism's specifications. Design concepts potentially delivering the required performance are then established. At this point, the design, noise, and responses should be clear, and defined within a search algorithm, e.g., DoE, GA, or Taguchi. We must then model the problem and execute the search. Depending on the specific approach, various forms of results relating to mean and variance are obtained. This should drive the initial design towards specifications. Very briefly, we demonstrate the application of this methodology in a case study.

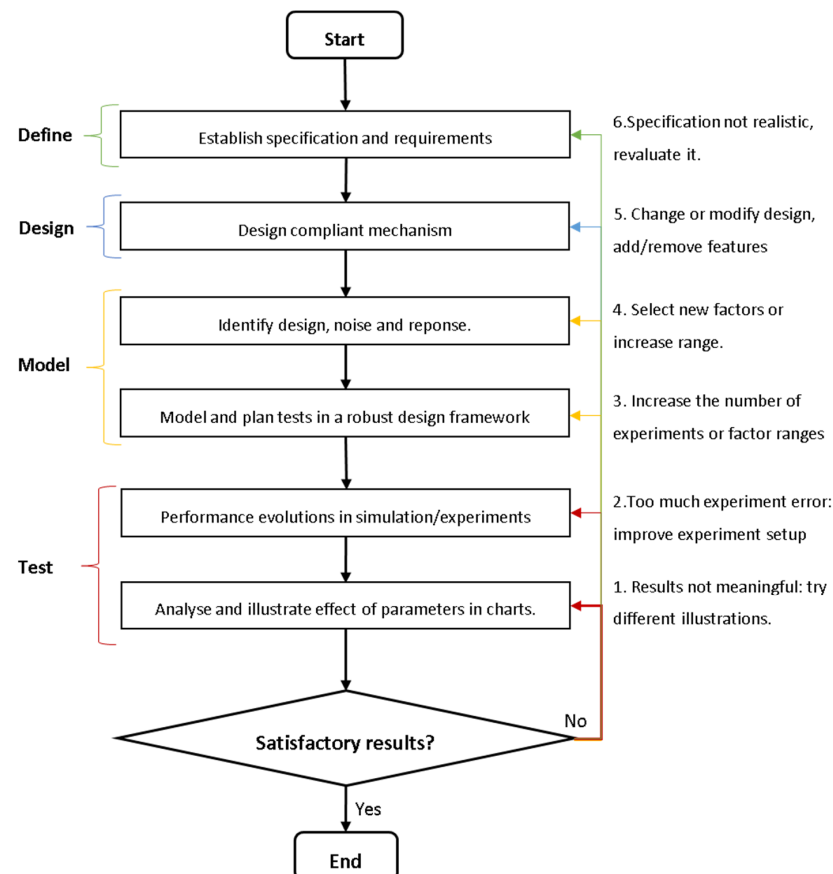


Figure 2. Flowchart of the proposed method for passive compliance design with RED.

2.2. Case Study

2.2.1. Problem Definition

Figure 3 shows the process and issue of coupling train fluid ports within our autonomous train fluid servicing system called CyberFluids [4,5,7,12]. We have introduced this system and investigated its performance in our previous work. We saw insertion forces of up to 600 N for 5 mm parallel misalignment. Considering that a human exerts between 50 and 100 N, we concluded this force is too large especially for such small misalignments. This work will be targeting less than 200 N for misalignments of 15 mm parallel and 5 degrees angular (based on the assumptions in Table 1). We seek a new end-effector design since we were not able to reach these values with the initial design; see the mission statement in Table 2.

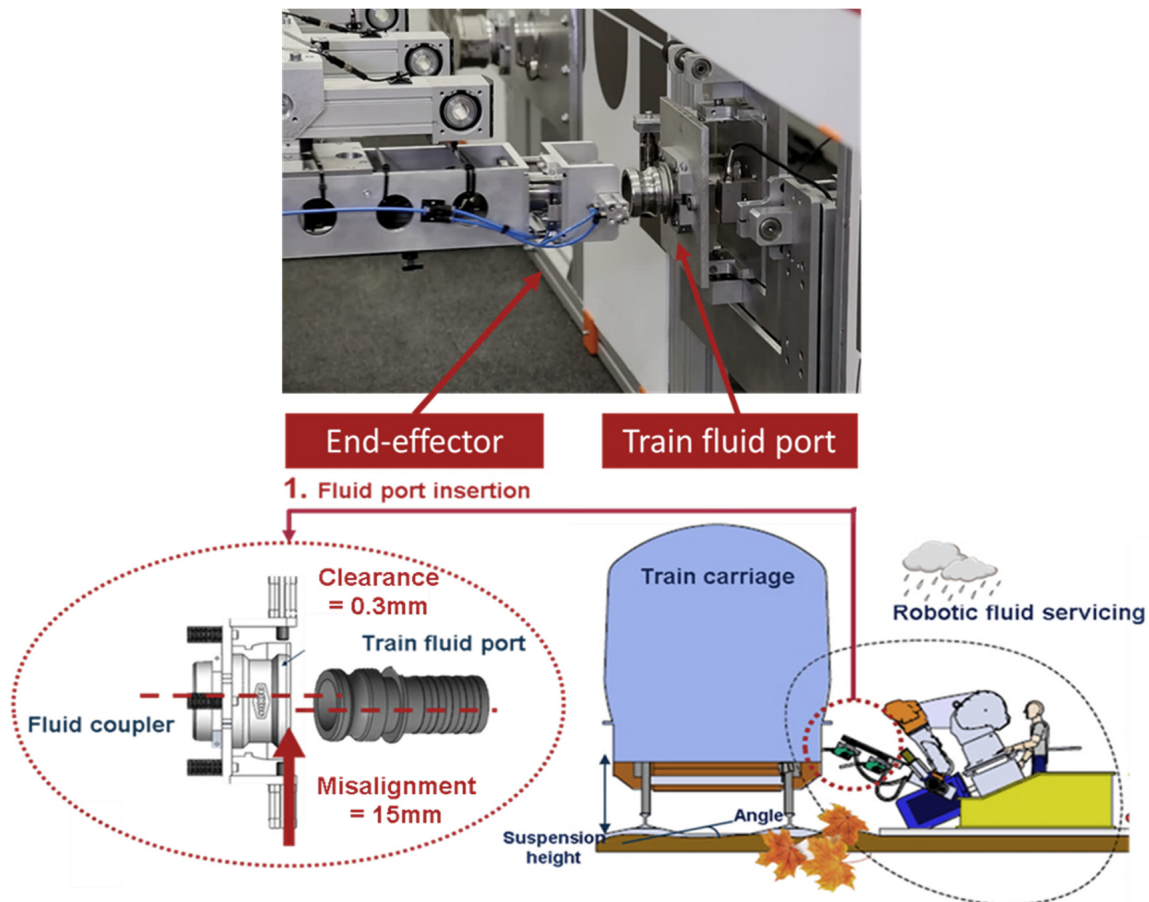


Figure 3. The robotic and autonomous train fluid coupling problem.

Table 1. The sources and amounts of misalignment possible in train maintenance.

| Source of Misalignment                                  | Linear (+/- mm) | Angular (+/- deg) |
|---------------------------------------------------------|-----------------|-------------------|
| Inaccuracy of robot mechanical movement                 | 1               | 0.5               |
| Inaccuracy of robot positioning relative to train       | 1               | 0.5               |
| Unintentional dimensional, i.e., due to wear tolerances | 3               | 1                 |
| Train suspension motion, e.g., due to wear or load      | 10              | 3                 |
| Sum of misalignments                                    | 15              | 5                 |

**Table 2.** Mission statement of the design purposes.

| Statement   | Description                                                                                                                                                                                                                       |
|-------------|-----------------------------------------------------------------------------------------------------------------------------------------------------------------------------------------------------------------------------------|
| Project     | 1. Compliant end-effector for coupling of hoses in train fluid servicing.                                                                                                                                                         |
| Benefit     | 1. Reduced cost and requirements on the robot side, i.e., a less complicated system with reduced degrees-of-freedom (DoFs) and payload. 2. Reduced operational forces for reduced health and safety risks.                        |
| Goal        | 1. End-effector designs with misalignment range of $\pm 15$ mm linear, 5 deg angular.<br>2. Reduce operating forces, to 150 N.<br>3. Incorporate compliant mechanisms to take advantage of their inherent benefits (i.e., costs). |
| Assumptions | 1. Robot is a Cartesian system like the CyberFluids system.<br>2. Dixon fluid ports are used in the end-effector, and train fluid ports are standardised using adapters.                                                          |

### 2.2.2. Design

Here, we will investigate a compliant end-effector with RCC capabilities [16]. The aforementioned work has found this to be useful in shaft-bearing insertions that are representable by a cylindrical PiH task. The fluid coupling process is very similar, but the geometry is different to a cylinder since extra grooves and geometric features are required for the latches and gaskets (see Figure 4). According to [8], geometric features such as chamfers and undercut grooves increase the misalignment range; hence, we believe these fluid ports can achieve large misalignments.

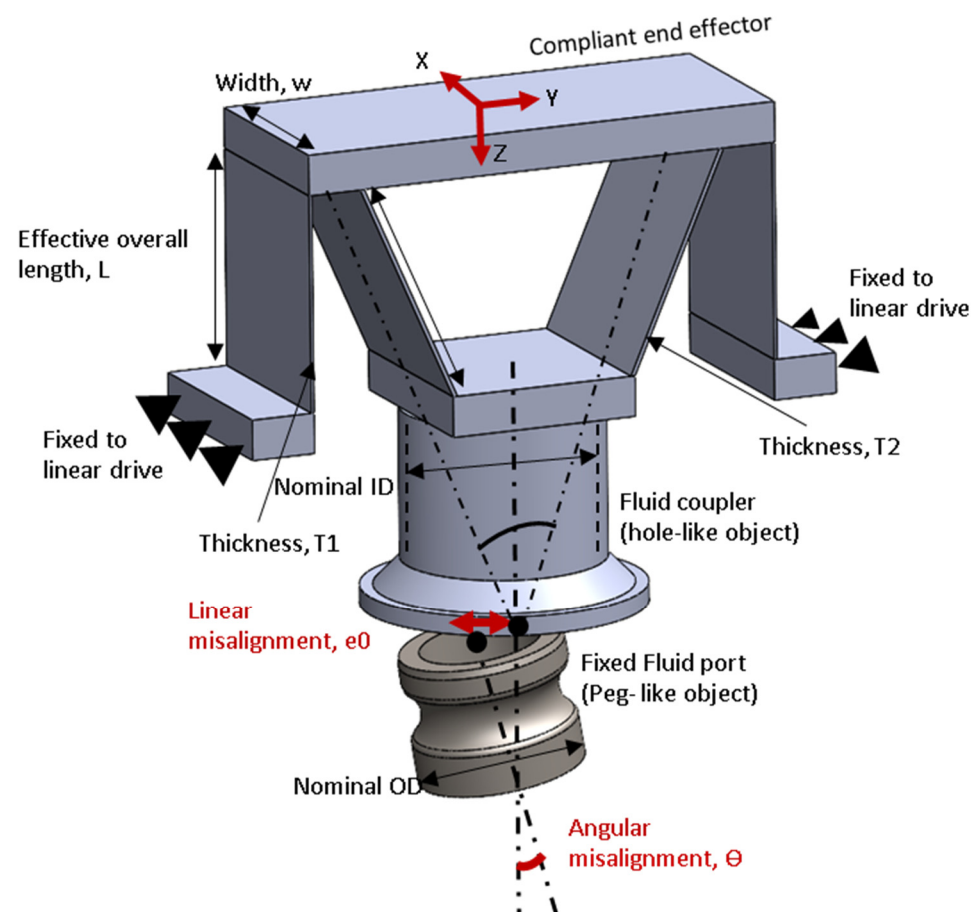


**Figure 4.** The 2-DoF RCC design and relevant parameters in the coupling of fluid ports.

Generally, an RCC device for cylindrical PiH shapes requires 4 DoFs (2 translational and 2 rotational). The insertion axis must be constrained and stiff to accommodate the insertion forces. Angular misalignment may be slightly augmented or corrected during chamfer crossing. This will also depend on the position of the RCC point. Typically (for

small misalignments), the stiffness of the angular stage is much higher than the linear stage to enable parallel travel across the chamfer; see Figure 5. The same figure presents two possible misalignment scenarios which may occur upon entry. There are four possible entry cases (in 2D); however, due to symmetry, analysis across two cases is sufficient.

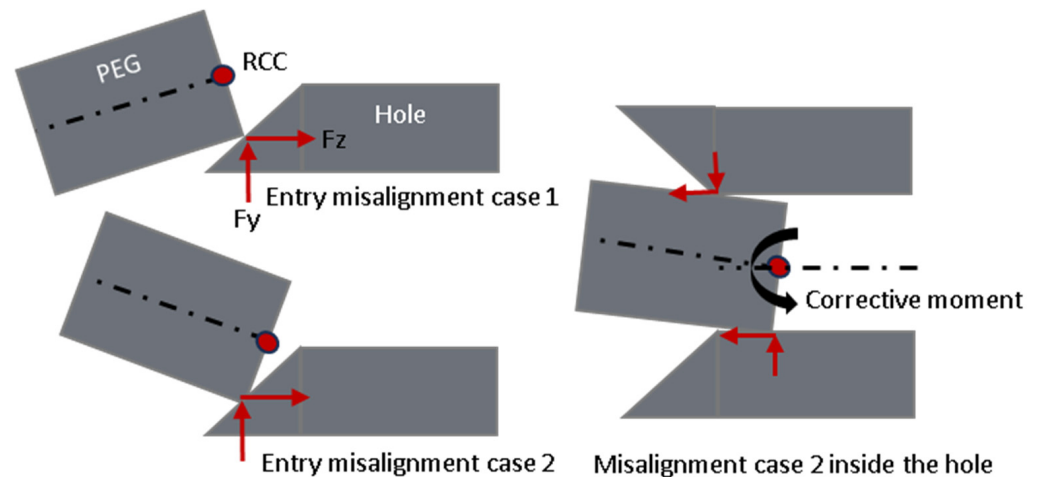


**Figure 5.** The insertion of the PiH and the effect of the contact force and RCC points.

The insertion and contact forces drive the motion of the peg during the coupling process. If the RCC point is far from the tip, the resulting turning moments due to the contact forces are larger. In one entry scenario in Figure 5, this causes more corrective motion, but in the other, it causes more angular misalignment. By setting the RCC point near the tip of the part, in both cases, the turning moment is equalised. Augmentation of the angular misalignment is reduced since the moment arm is minimised for both cases. When the peg is inside the hole there is more chance of wedging and jamming, a similar corrective motion is achieved for this scenario. For the case where the hole is being carried by the end-effector, the RCC can be set halfway through the chamfer to achieve similar effects.

A remote centre of motion (RCM) can be attained through various linkage arrangements [37]. For cross-flexure-based compliant mechanisms, beams arranged with an instantaneous centre of rotation create an RCC effect, as constraint lines coincide at the point of rotation. Essentially, by constraining all irrelevant DoFs, RCC is attained. For this academic endeavour, we will use one of the 2-DoF modules (Figure 4) required as part of the complete 4-DoF end-effector. The results obtained for this module will translate across to an identical module constituting the end-effector.

### 2.2.3. Modelling

We use a PRBM approach to compare with FEA with LS Dyna. The first step is to convert this compliant mechanism to its rigid body equivalent. According to the PRBM method [15], the beams comprising the parallel stage can be considered as fixed-guided beams (see Figure 6) since the angles between the motion stage and beam-ends do not vary relative to the fixed stage. Since both beams are identical, all four pseudo-springs on the parallel stage have the same stiffness, given by

$$K_p = 2\gamma K_\varnothing \frac{EI}{l} \quad (7)$$

where  $K_\varnothing$  and  $\gamma$  are parametric coefficients known as the stiffness coefficient and characteristic radius factor, respectively. These parameters depend on the loading conditions and are

typically updated during the analysis. However, for a large range of loading conditions, these values can be nearly constant, given as [15]

$$\gamma = 0.852144 - 0.0182867n ; \quad (8)$$

for  $-1.8316 < n < 0.5$

$$K_\theta = 2.654855 - 0.0509896n + 0.0126749n^2 - 0.00142039n^3 + 0.00000584525n^4 ; \quad (9)$$

for  $-1 < n < 10$

where  $n$  is the load factor, which is the proportion of lateral force in the axial direction on the beam.  $n$  is positive for compressive loads and zero where there is only a lateral force present.  $\gamma$  also reveals the position of the torsional springs (and revolute joints) along the beam. At this point, the rigid body equivalent of the parallel stage is fully defined.

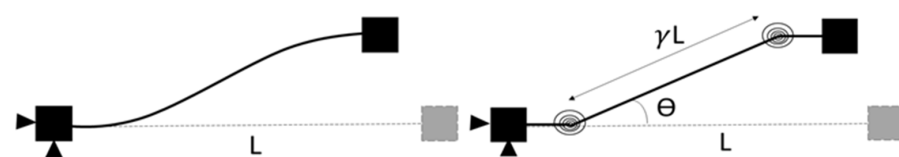


**Figure 6.** The compliant (left) and equivalent rigid body (right) of a guided beam.

For the angular stage, we follow the 3R model [38], where the torsional stiffness of the pseudo-springs is given by

$$K_i = k_i c_i \left( \frac{EI}{L} \right) \quad (10)$$

Each beam has 3 springs with stiffness  $K_i$  at locations  $\gamma_i$  [38]. The rigid equivalent of the mechanism and PiH problem is modelled (see Figure 7) using a numerical rigid body solver, in our case SolidWorks Motion analysis. This package allows for the addition of the following simulation elements and settings that we have used to model the problem.

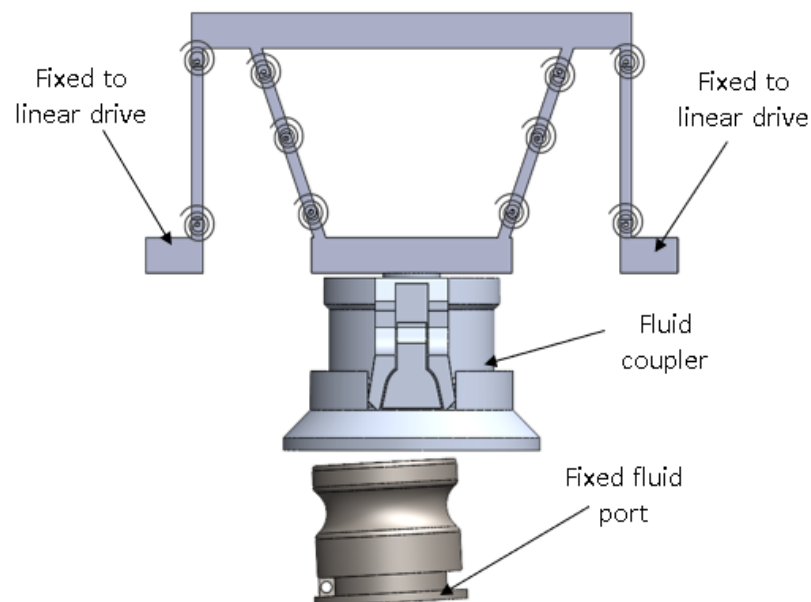


**Figure 7.** PRBM model set up in SolidWorks Motion analysis.

- Linear motor: This is the robot arm which follows a linear path at a constant speed.
- Solid-body contacts: This is defined between the peg and the hole. We have found that increasing the stiffness and damping of the contact provides more accurate results; for fluid coupling we use 200,000 N/mm and 100 Ns/mm.

- Contact resolution is set to “precise contact”, with an integrator accuracy of 0.001 to ensure analytically sound results. The integrator used is WSTIFF, which responds better to abrupt changes (e.g., impact and contact separation).
- The number of frames per second is set to 50 for all insertions below 5 mm/s; for higher speeds, >5 mm/s and <15 mm/s, we use 100 FPS.
- SolidWorks motion analysis encourages no redundant DoFs, resulting from the mating of components to provide accurate force results. Redundant mates may be replaced with “bushings” with high stiffness, typically in the order of  $10 \times 10^7$  N/mm. This stiffness is many orders of magnitude greater than the compliance of the mechanism, hence it will not induce noticeable error.

The FEA simulation package used is LS-Dyna, which is available with the Ansys workbench. This explicit dynamic approach is more suitable, since rigid body translations are resolved and there are no convergence iterations in solving the equation of motion (Formula (11)). The caveat is that there are difficulties in meshing and controlling the time steps for feasible run times. This is due to the time-step calculations being based on the critical Courant number (Formula (12)). This condition ensures that stress-wave propagation through the elements is captured in the simulation. Time steps beyond that cause instabilities and invalid results. There is no stress wave through an ideally rigid body. Thus, the time steps are independent of the rigid body mesh, so refinement can be allocated to these important contact regions with little added expense. Figure 8 is a typical setup used for modelling fluid coupling. Ansys quad shell elements are used for the compliant mechanism and tetrahedral solid elements are used for the fluid couplers. The boundary conditions are fixed supports (zero displacements) at the end-effector/robot mount point and applied displacements (remote displacement option) at the fluid port. Contact is defined between all outer surfaces of the fluid port and all inner surfaces of the coupler. The contact formulation is augmented Lagrange. The coupler is attached to the motion stage of the end-effector with rigid constraint joints. Connecting bodies are bonded with mesh adjustments which ensure common nodes between connecting surfaces. Materials are defined as isotropic. For both the FEA and PRBM models, friction is maintained as a constant value.

$$\mathbf{M} \mathbf{U}''(t) + \mathbf{C} \mathbf{U}'(t) + \mathbf{K} \mathbf{U}(t) = \mathbf{F}(t) \quad (11)$$

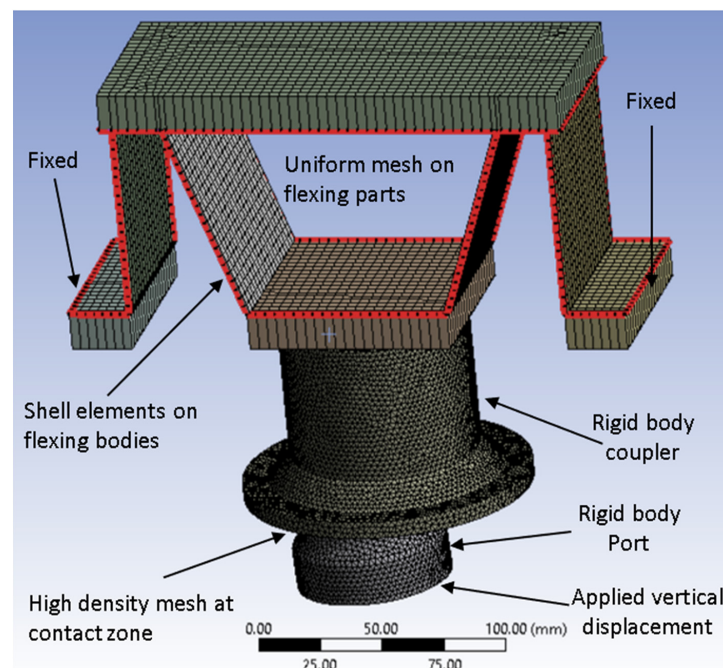


Figure 8. FEA model setup in the LS-Dyna Ansys workbench.

In the above formulation,  $M$ ,  $C$ , and  $K$  are, respectively, the mass, damping, and stiffness matrices.  $F$  is the loads,  $U$  is the displacements, and  $t$  is time.

$$t_{crit} = \frac{fL}{C} \tag{12}$$

where  $f$  is a numerical safety/scale factor and takes values of 0–1,  $L$  is the characteristic length of the smallest flexible element, and  $C$  is the speed of sound through the flexible material.

#### 2.2.4. RED Plan

In the following, we use a Taguchi approach, since it requires minimum statistical effort with a small number of runs for 2 design factors and 2 noise factors. The 2 noise factors are linear and angular misalignments. Each factor at 2 levels yields a total of 16 runs. The aim is to identify the most suitable configuration that yields the best mean performance with the least variability for a prototype end-effector. Tables 3 and 4 discuss the details for each run. We consider high (1) and low (0) settings to correspond to the top and bottom of the range bounds, respectively. Taguchi’s signal-to-noise ratio (SNR) aims to indicate the desirable solution; in our case it translates to the “smaller is better” formula:

$$\frac{S}{N} = -10 \log \left( \frac{\sum_{i=1}^n (Y_i^2)}{n} \right) \tag{13}$$

**Table 3.** Experiment variables and their settings.

| Experiment Variable  | Symbol   | Model Comparison Study | RED Study   | Units |
|----------------------|----------|------------------------|-------------|-------|
| Overall length       | L        | 0.9                    | 0.7 to 0.11 | N/mm  |
| Thickness ratio      | T2/T1    | 1.2                    | 1.2 to 1.5  | -     |
| Linear misalignment  | $e_0$    | 5                      | 5 to 15     | mm    |
| Angular misalignment | $\Theta$ | 4                      | –5 to 5     | deg   |
| Thickness            | T1       | 2                      | 2           | mm    |
| Friction coefficient | F        | 0.2                    | 0.15        | -     |
| Nominal ID           | ID       | 63                     | 63          | mm    |
| Nominal OD           | OD       | 63.85                  | 63.85       | mm    |
| Insertion speed      | V        | 5                      | 10          | mm/s  |
| Elastic modulus      | E        | 3                      | 2.6         | GPa   |

**Table 4.** Results and configuration of the Taguchi plan.

| Config # |   |          |     |     |       |       | $\bar{Y}$ | $Y_{SD}$ | S/N    |
|----------|---|----------|-----|-----|-------|-------|-----------|----------|--------|
|          | L | T2/T1    | Y1  | Y2  | Y3    | Y4    |           |          |        |
|          |   | $e_0$    | 1   | 1   | 0     | 0     |           |          |        |
|          |   | $\Theta$ | 1   | 0   | 1     | 0     |           |          |        |
| <b>1</b> | 1 | 1        | 91  | 116 | 100   | 107.5 | 103.63    | 10.66    | –35.01 |
| <b>2</b> | 1 | 0        | 103 | 69  | 54.5  | 61    | 71.88     | 21.58    | –32.85 |
| <b>3</b> | 0 | 1        | 243 | 315 | 250.5 | 281   | 272.38    | 32.83    | –42.73 |
| <b>4</b> | 0 | 0        | 255 | 237 | 152   | 178   | 205.50    | 48.51    | –42.21 |

The design factors selected for this study are the overall effective length  $L$  and the thickness ratio of the angular and parallel beams. Please refer back to Figure 4 for an illustration and nomenclature. Note that parameters such as the effective overall length,  $L$ , and width,  $w$ , are shared between the linear and angular stages. That is,  $L$  geometrically constrains  $L_a$ . The RCC point is kept in the middle of the funnel, 10 mm outside the the mouth of the hole. We measure the performance as the maximum insertion force ( $Y = F_z$ ) using the PRBM model.

### 3. Results

Figure 9 shows the comparison of the FEA and PRBM models in estimating the insertion force. A generally good match is observed, with the two lines almost overlaid.

The maximum difference between the results during the whole coupling process is up to 12%.

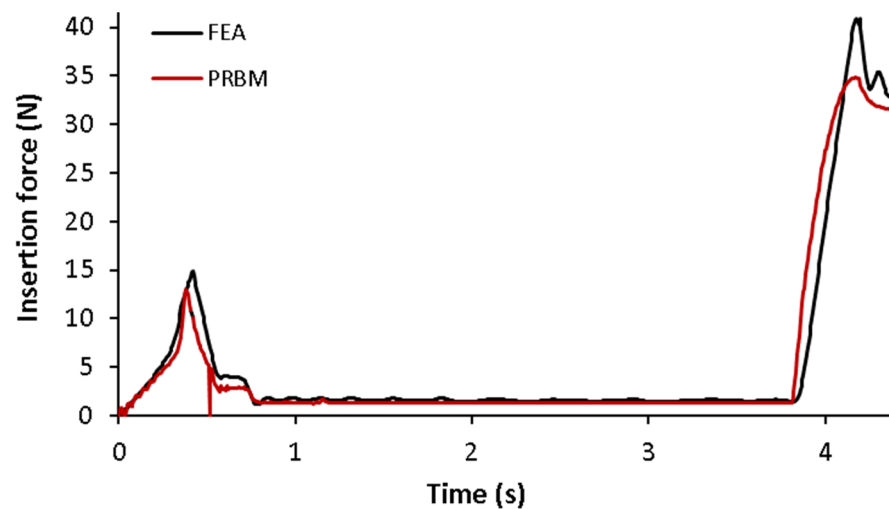


**Figure 9.** Comparison of PRBM and FEA in measuring the insertion force during the coupling process.

The PRBM simulation takes ~10 min with an Intel I7 H series, RAM of 16 GB and 6 GB GPU. For the FEA simulation with a time step of  $\sim 2.5 \times 10^{-7}$ , the simulation time is ~35 h on the same PC.

Table 4 shows the configurations and results of the Taguchi experiments that were performed using the PRBM model. We can see that config1 has the lowest SD while config2 results in the lowest mean. Config2 results in the best SNR value, indicating that it is potentially the best configuration.

Figures 10 and 11 provide further insight into the mean effect of design factor levels on the mean and standard deviation of the insertion force. The way we obtained this figure was by averaging the observed values for the given design factor level. We can see that increasing L reduces the insertion forces and the opposite is true for T2/T1. Increasing both design factors results in a reduction in the standard deviation, with L being more effective at this. Looking at the results in Table 4, configuration 2 has the best SNR and the best mean performance. However, a 50% lower standard deviation is achieved in configuration 1. This is at the cost of a 43% decrease in the mean performance. We can also see that the SNRs for configurations 1 and 2 are quite close. Thus, if the reduction in mean performance is feasible, then configuration 1 is a more robust design. Accordingly, in the Taguchi approach, it is always best practice to evaluate the mean and standard deviation alongside the SNR for more informed decisions. We can confirm that higher values of T2/T1 reduce the standard deviation but decrease the performance (higher force). For the given experimental range of variables, we can conclude that both T2/T1 and L have a high impact on both the standard deviation and the mean. Finally, the obtained results facilitate actuator sizing for insertion. We can estimate the required payload  $F_{actuator}$  by assuming a Gaussian distribution:

$$F_{actuator} = (\bar{Y} + 3Y_{SD}) \quad (14)$$

Common practice is to use the above “three sigma” rule to ensure a 99.73% chance that the maximum possible force is accounted for. We should also allow up to 10% due to simulation inaccuracies and up to 10% oversizing. Hence, as an example, for design configuration #1, we need a robot payload of at least 135.61 N, which can be rounded up to 150 N. We selected this configuration for our prototyping since it has a lower standard deviation, and the actuator force is feasible for our applications.

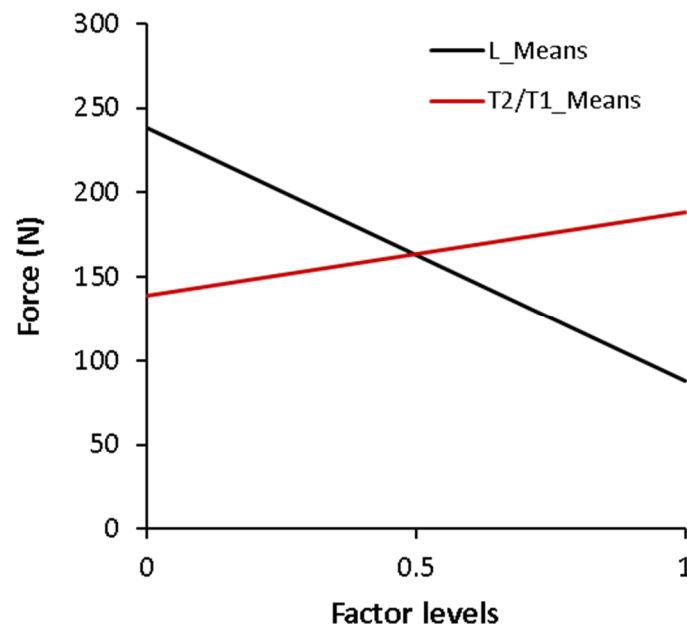


Figure 10. Plot showing the effect of design factor levels on the mean of the maximum insertion force.

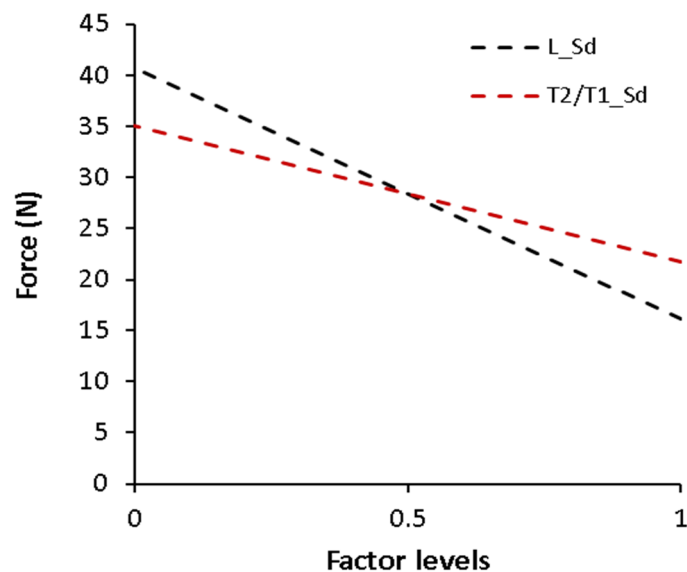


Figure 11. Plot showing the effect of design factor levels on the SD of the maximum insertion force.

#### 4. Discussions and Conclusions

A special kind of flexibility (compliance) is required to complete certain automated tasks in railway vehicle maintenance, where an uncertain contact occurs between the robot and the train. We can achieve compliance through the mechanical design of the robot and/or workpiece interface on the train. In this work, we developed and shared various modelling and analysis tools that enable robust and effective passive compliance design. In particular, for the development of compliant end-effectors in train fluid servicing. Nonetheless, our methodology stands as a general and novel take on the problem relatable to many applications. Some limitations of our work include the assumption of cheap-to-implement models; it can be argued that as the numbers of design and noise factors increase, the number of performance evaluations increase significantly to satisfy the expanded design space. Furthermore, the selection of the design factor ranges is also slightly uncertain since it will depend on the experience and intuition of the designer. Thus, these factors should be considered upon taking up the proposed approach.

The particular end-effector design studied proved more successful than our previous development for train fluid servicing, reducing the maximum insertion forces by around 300% while increasing the misalignment range three-fold. Furthermore, we have demonstrated how to efficiently model passive compliance problems with PRBM, which is 14,000% faster than classic FEA modelling. These are significant achievements facilitated by our proposed methodology and modelling approach, which considers previously overlooked practical aspects of design, large deformations, and complex geometries of interacting components.

The rail industry may benefit from this line of work in the development of:

1. Compliant robotics for autonomous train fluid servicing in a retrofittable manner;
2. New standardised fluid port interfaces and adaptors for robot-friendly maintenance;
3. New interfaces and compliant robotics for other tasks, e.g., shoe gear replacement;
4. Robotic rolling stock manufacturing.

Overall, the rail industry will benefit significantly by incorporating compliant end-effectors in the future design of trains and autonomous systems for maintenance. We have shown how to reduce the robot payload and precision requirements, resulting in much more economical solutions for mass-scale applications. However, encouraging train manufacturers to incorporate very small design changes which enable robot-friendly maintenance will further reduce robot requirements and costs. In terms of servicing fluids, this translates to easily accessible fluid ports, and standardised fluid ports and coupling interfaces, that we assumed to be the camlock coupling. In the future, there will be more detailed considerations of fluid port requirements and standardised interfaces for rolling stock maintenance. Perhaps this is a subject for our future work.

**Author Contributions:** K.E. is the lead author responsible for synthesising the paper, its propositions, and novelties. The work presented here is the subject of his PhD thesis. M.W. has supervised this work and provided significant effort for the development of this paper. C.M. has provided valuable support to facilitate our research. All authors have read and agreed to the published version of the manuscript.

**Funding:** We especially thank and acknowledge the funding and support from the Rail Safety and Standards Board (RSSB), under contract RSSB 2675, and from EPSRC Impact Acceleration Account, under the Grant No. EP/X525510/1.

**Conflicts of Interest:** The authors declare no conflict of interest. The funders had no role in the design of the study; in the collection, analyses, or interpretation of data; in the writing of the manuscript; or in the decision to publish the results.

## References

1. Rail Delivery Group. *Long Term Passenger Rolling Stock Strategy for the Rail Industry*; Rail Delivery Group: London, UK, 2018; Available online: [https://www.raildeliverygroup.com/files/Publications/2018-03\\_long\\_term\\_passenger\\_rolling\\_stock\\_strategy\\_6th\\_ed.pdf](https://www.raildeliverygroup.com/files/Publications/2018-03_long_term_passenger_rolling_stock_strategy_6th_ed.pdf) (accessed on 23 October 2023).
2. Hawkes, E.W.; Cutkosky, M.R. Design of Materials and Mechanisms for Responsive Robots. *Annu. Rev. Control Robot. Auton. Syst.* **2018**, *1*, 359–384. [[CrossRef](#)]
3. Wang, T. Editorial Overview: Advances in Robotic Technologies. *Engineering* **2018**, *4*, 433–434. [[CrossRef](#)]
4. Atherton, M.; Hill, S.; Harrison, D.; Ajovalasit, M. Economic and Technical Feasibility of a Robotic Autonomous System for Train Fluid Servicing. *Proc. Inst. Mech. Eng. Part F J. Rail Rapid Transit* **2020**, *234*, 338–350. [[CrossRef](#)]
5. Eshraghi, K.; Jiang, P.; Suraci, D.; Atherton, M. Preliminary Study on End-Effector Compliance in Automated Fluid Coupling for Trains. In Proceedings of the Thirteenth International Tools and Methods of Competitive Engineering, Dublin, Ireland, 11–15 May 2020.
6. Guastella, D.C.; Muscato, G. Learning-Based Methods of Perception and Navigation for Ground Vehicles in Unstructured Environments: A Review. *Sensors* **2020**, *21*, 73. [[CrossRef](#)] [[PubMed](#)]
7. Hill, S.A.; Atherton, M.; Ajovalasit, M.; Harrison, D. *Robust Automated Servicing of Passenger Trains-Fluids*; Brunel University: Uxbridge, UK, 2017.
8. Daniel, E. *Whitney Mechanical Assemblies Their Design, Manufacture, and Role in Product Development*; Oxford University Press: Oxford, UK, 2004.
9. Jiang, J.; Bian, C.; Ke, Y. A New Method for Automatic Shaft-Hole Assembly of Aircraft Components. *Assem. Autom.* **2017**, *37*, 64–70. [[CrossRef](#)]

10. Flores-Abad, A.; Ma, O.; Pham, K.; Ulrich, S. A Review of Space Robotics Technologies for On-Orbit Servicing. *Prog. Aerosp. Sci.* **2014**, *68*, 1–26. [[CrossRef](#)]
11. Ogilvie, A.; Allport, J.; Hannah, M.; Lymer, J. Autonomous Satellite Servicing Using the Orbital Express Demonstration Manipulator System. In Proceedings of the 9th International Symposium on Artificial Intelligence, Robotics and Automation in Space, Beijing, China, 19–21 October 2020.
12. Eshraghi, K.; Jiang, P.; Suraci, D.; Atherton, M. Preliminary Study of End-Effector Compliance for Reducing Insertion Force in Automated Fluid Coupling for Trains. *JID* **2020**, *24*, 139–161. [[CrossRef](#)]
13. Xu, J.; Hou, Z.; Liu, Z.; Qiao, H. Compare Contact Model-Based Control and Contact Model-Free Learning: A Survey of Robotic Peg-in-Hole Assembly Strategies. *arXiv* **2019**, arXiv:1904.05240.
14. Wang, W.; Loh, R.N.; Gu, E.Y. Passive Compliance versus Active Compliance in Robotbased Automated Assembly Systems. *Ind. Robot.* **1998**, *25*, 48–57, ISSN 0143-991X. [[CrossRef](#)]
15. Howell, L.L.; Olsen, B.M.; Spencer, P. *Handbook of Compliant Mechanisms*; Wiley: Hoboken, NJ, USA, 2013.
16. Whitney, D.E. Quasi-Static Assembly of Compliantly Supported Rigid Parts. *J. Dyn. Syst. Meas. Control* **1982**, *104*, 65–77. [[CrossRef](#)]
17. Whitney, D.E.; Rourke, J.M. Mechanical Behavior and Design Equations for Elastomer Shear Pad Remote Center Compliances. *J. Dyn. Syst. Meas. Control* **1986**, *108*, 223–232. [[CrossRef](#)]
18. Zhao, Y.; Chen, K.; Yu, J.; Huang, S. Design of a Parallel Compliance Device with Variable Stiffness. *Proc. Inst. Mech. Eng. Part C J. Mech. Eng. Sci.* **2021**, *235*, 94–107. [[CrossRef](#)]
19. Parvari Rad, F.; Verthey, R.; Berselli, G.; Parenti-Castelli, V. Design and Stiffness Evaluation of a Compliant Joint with Parallel Architecture Realizing an Approximately Spherical Motion. *Actuators* **2018**, *7*, 20. [[CrossRef](#)]
20. Ding, B.; Li, Y. Design and Analysis of a Decoupled XY Micro Compliant Parallel Manipulator. In Proceedings of the 2014 IEEE International Conference on Robotics and Biomimetics (ROBIO 2014), Bali, Indonesia, 5–10 December 2014; pp. 1898–1903.
21. Dan, W.; Rui, F. Design and Nonlinear Analysis of a 6-DOF Compliant Parallel Manipulator with Spatial Beam Flexure Hinges. *Precis. Eng.* **2016**, *45*, 365–373. [[CrossRef](#)]
22. Shintake, J.; Cacucciolo, V.; Floreano, D.; Shea, H. Soft Robotic Grippers. *Adv. Mater.* **2018**, *30*, 1707035. [[CrossRef](#)]
23. Petković, D.; Pavlović, N.; Shamshirband, S.; Badrul Anuar, N. Development of a New Type of Passively Adaptive Compliant Gripper. *Ind. Robot Int. J.* **2013**, *40*, 610–623. [[CrossRef](#)]
24. Sun, Y.; Liu, Y.; Pancheri, F.; Lueth, T.C. LARG: A Lightweight Robotic Gripper With 3-D Topology Optimized Adaptive Fingers. *IEEE/ASME Trans. Mechatron.* **2022**, *27*, 2026–2034. [[CrossRef](#)]
25. Burgner-Kahrs, J.; Rucker, D.C.; Choset, H. Continuum Robots for Medical Applications: A Survey. *IEEE Trans. Robot.* **2015**, *31*, 1261–1280. [[CrossRef](#)]
26. Noh, Y.; Han, S.; Gawenda, P.; Li, W.; Sareh, S.; Rhode, K. A Contact Force Sensor Based on S-Shaped Beams and Optoelectronic Sensors for Flexible Manipulators for Minimally Invasive Surgery (MIS). *IEEE Sens. J.* **2020**, *20*, 3487–3495. [[CrossRef](#)]
27. Sanchez-Villamañan, M.D.C.; Gonzalez-Vargas, J.; Torricelli, D.; Moreno, J.C.; Pons, J.L. Compliant Lower Limb Exoskeletons: A Comprehensive Review on Mechanical Design Principles. *J. NeuroEngineering. Rehabil.* **2019**, *16*, 55. [[CrossRef](#)]
28. Polygerinos, P.; Wang, Z.; Galloway, K.C.; Wood, R.J.; Walsh, C.J. Soft Robotic Glove for Combined Assistance and At-Home Rehabilitation. *Robot. Auton. Syst.* **2015**, *73*, 135–143. [[CrossRef](#)]
29. Sturges, R.H.; Laowattana, S. Design of an Orthogonal Compliance for Polygonal Peg Insertion. *J. Mech. Des.* **1996**, *118*, 106–114. [[CrossRef](#)]
30. Kamnik, R.; Rodič, G.; Mihelj, M.; Bajd, T. Automation of the Car Battery Lid Assembly Operation. *Robot. Comput.-Integr. Manuf.* **2001**, *17*, 435–446. [[CrossRef](#)]
31. Jain, R.K.; Majumder, S.; Dutta, A. SCARA Based Peg-in-Hole Assembly Using Compliant IPMC Micro Gripper. *Robot. Auton. Syst.* **2013**, *61*, 297–311. [[CrossRef](#)]
32. Southern, W.R.; Lyons, C.G. The Study of a Passive Accommodation Device in Robotic Insertion Processes. *J. Mater. Process. Technol.* **2002**, *124*, 261–266. [[CrossRef](#)]
33. Atherton, M.A.; Bates, R.A. Robust Optimization of Cardiovascular Stents: A Comparison of Methods. *Eng. Optim.* **2004**, *36*, 207–217. [[CrossRef](#)]
34. Dean, A.; Voss, D. *Design and Analysis of Experiments*; Wiley: Hoboken, NJ, USA, 2012.
35. Arvidsson, M.; Gremyr, I. Principles of Robust Design Methodology. *Qual. Reliab. Engng. Int.* **2008**, *24*, 23–35. [[CrossRef](#)]
36. Eppinger, S.D.; Ulrich, K. *Product Design and Development*, 6th ed.; McGraw Hill: New York, NY, USA, 2015.
37. Zong, G.; Pei, X.; Yu, J.; Bi, S. Classification and Type Synthesis of 1-DOF Remote Center of Motion Mechanisms. *Mech. Mach. Theory* **2008**, *43*, 1585–1595. [[CrossRef](#)]
38. Chen, G.; Xiong, B.; Huang, X. Finding the Optimal Characteristic Parameters for 3R Pseudo-Rigid-Body Model Using an Improved Particle Swarm Optimizer. *Precis. Eng.* **2011**, *35*, 505–511. [[CrossRef](#)]

**Disclaimer/Publisher’s Note:** The statements, opinions and data contained in all publications are solely those of the individual author(s) and contributor(s) and not of MDPI and/or the editor(s). MDPI and/or the editor(s) disclaim responsibility for any injury to people or property resulting from any ideas, methods, instructions or products referred to in the content.